Gearbox Reliability Collaborative Phase 3 Gearbox 3 Test Report

Jonathan Keller and Robb Wallen
National Renewable Energy Laboratory

NREL is a national laboratory of the U.S. Department of Energy
Office of Energy Efficiency & Renewable Energy
Operated by the Alliance for Sustainable Energy, LLC

This report is available at no cost from the National Renewable Energy Laboratory (NREL) at www.nrel.gov/publications.

Technical Report
NREL/TP-5000-67612
February 2017

Contract No. DE-AC36-08GO28308

NREL
NATIONAL RENEWABLE ENERGY LABORATORY

Gearbox Reliability Collaborative Phase 3 Gearbox 3 Test Report

Jonathan Keller and Robb Wallen
National Renewable Energy Laboratory

Prepared under Task No. WE16.5A02

NREL is a national laboratory of the U.S. Department of Energy
Office of Energy Efficiency & Renewable Energy
Operated by the Alliance for Sustainable Energy, LLC

This report is available at no cost from the National Renewable Energy Laboratory (NREL) at www.nrel.gov/publications.

National Renewable Energy Laboratory
15013 Denver West Parkway
Golden, CO 80401
303-275-3000 • www.nrel.gov

Technical Report
NREL/TP-5000-67612
February 2017

Contract No. DE-AC36-08GO28308

This report is available at no cost from the National Renewable Energy Laboratory (NREL) at www.nrel.gov/publications.

Available electronically at SciTech Connect http:/www.osti.gov/scitech

Available for a processing fee to U.S. Department of Energy and its contractors, in paper, from:

U.S. Department of Energy
Office of Scientific and Technical Information
P.O. Box 62
Oak Ridge, TN 37831-0062
OSTI http://www.osti.gov
Phone: 865.576.8401
Fax: 865.576.5728
Email: reports@osti.gov

Available for sale to the public, in paper, from:

U.S. Department of Commerce
National Technical Information Service
5301 Shawnee Road
Alexandria, VA 22312
NTIS http://www.ntis.gov
Phone: 800.553.6847 or 703.605.6000
Fax: 703.605.6900
Email: orders@ntis.gov

Cover Photos by Dennis Schroeder: (left to right) NREL 26173, NREL 18302, NREL 19758, NREL 29642, NREL 19795.

NREL prints on paper that contains recycled content.

Acknowledgments

This work was supported by the U.S. Department of Energy (DOE) under Contract No. DE-AC36-08GO28308 with the National Renewable Energy Laboratory. Funding for the work was provided by the DOE Office of Energy Efficiency and Renewable Energy, Wind Energy and Water Power Technologies Office.

List of Acronyms

CRB	cylindrical roller bearing
DAS	data acquisition system
GRC	Gearbox Reliability Collaborative
HSS	high-speed shaft
Hz	hertz
kN	kilonewton
kNm	kilonewton meter
kW	kilowatt
LSS	low-speed shaft
mV/V	millivolts per volt
MW	megawatt
NREL	National Renewable Energy Laboratory
NTL	nontorque load
NWTC	National Wind Technology Center
TRB	tapered roller bearing

Table of Contents

List of Figures

List of Tables

1 Introduction and Background

Many gearboxes in wind turbines do not achieve their expected design life [1]; they do, however, commonly meet or exceed the design criteria specified in current standards in the gear, bearing, and wind turbine industry as well as third-party certification criteria. The cost of gearbox replacements and rebuilds, as well as the downtime associated with these failures, increases the cost of wind energy. In 2007, the U.S. Department of Energy established the National Renewable Energy Laboratory (NREL) Gearbox Reliability Collaborative (GRC). Its goals are to understand the root causes of premature gearbox failures and to improve their reliability [2]. The GRC is examining a hypothesis that the gap between design-estimated and actual wind turbine gearbox reliability is caused by underestimation of loads, inaccurate design tools, the absence of critical elements in the design process, or insufficient testing.

The GRC uses a combined gearbox testing, modeling, and analysis approach. To date, it has focused on a 750-kilowatt (kW) drivetrain, including the dedicated design of a nonproprietary gearbox with cylindrical roller bearings (CRBs) in the planetary section. Two of these gearboxes, GB1 and GB2, were manufactured and tested. Phase-1 and Phase-2 testing focused on planetary section load-sharing characteristics [2]. A major finding was the detrimental effect of rotor nontorque loads (NTLs) on load sharing, predicted fatigue life in high-torque conditions, and the risk of bearing skidding in low-torque conditions [3]. The GRC has disseminated engineering drawings, gearbox models, test data, and results [4], which have facilitated improvements to gearbox design standards and associated modeling tools. More recently, additional dynamometer tests in Phase 3 were conducted [5,6] with additional instrumentation on the high-speed shaft (HSS) and its locating tapered roller bearing (TRB) pair [7,8]. The objective of these tests was to assess HSS TRB load-sharing characteristics with a misaligned generator [9-11] and the potential for roller slipping during transient and grid loss events [12,13].

Simultaneous with the Phase-3 testing on the original GRC gearbox design, the GRC gearbox was redesigned to improve its load-sharing characteristics and predicted fatigue life. This new gearbox is referred to as GB3. The redesign was led by Romax Technology with contributions from Powertrain Engineers and The Timken Company (hereafter referred to as Timken). The most important aspect of the redesign was to replace the CRBs with preloaded TRBs in the planetary section [14-17], resulting in a projected increase of three times the planetary section fatigue life compared to the previous design [18]. Brad Foote Gearing assembled the gearbox.

This report describes the recently completed tests of GRC GB3 in the National Wind Technology Center (NWTC) dynamometer and documents any modifications to the original test plan [19]. In this manner, it serves as a guide for interpreting the publicly released data sets [20] with brief analyses to illustrate the data. The primary test objective was to measure the planetary load-sharing characteristics in the same conditions as the original GRC gearbox design. If the measured load-sharing characteristics are close to the design model, the projected improvement in planetary section fatigue life and the efficacy of preloaded TRBs in mitigating the planetary bearing fatigue failure mode will have been demonstrated. Detailed analysis of that test objective will be presented in subsequent publications.

2 Test Article

The GRC drivetrain was originally designed for a stall-controlled, three-bladed turbine with a rated power of 750 kW [2]. The drivetrain generates electricity at two main shaft speeds: 14.7 rpm and 22.1 rpm. The gearbox ratio of 81.491 converts these main shaft speeds to generator speeds of 1,200 rpm and 1,800 rpm. The drivetrain design follows a conventional configuration in which the main bearing and main shaft, gearbox, and generator are mounted to the bed plate as shown in Figure 1. The main shaft is connected to the gearbox via a shrink disk and the gearbox is connected to the generator via a flexible coupling. The gearbox is mounted with a three-point configuration in which forces are reacted mostly at the main bearing, whereas rotor moments and torque loads are transferred to the bed plate through two torque arms.

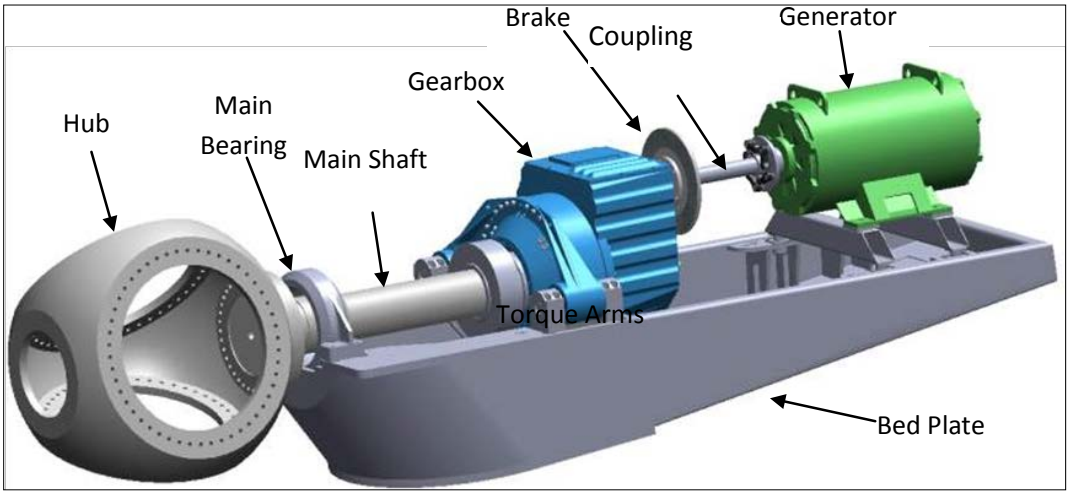

Figure 1. Drivetrain configuration

The GRC gearboxes are composed of one low-speed planetary stage with three planet gears and two parallel shaft stages as shown in Figure 2. The housing components of the original Jahnel-Kestermann PSC 1000-48/60 commercial gearboxes were retained, but the majority of the internal components were redesigned and newly manufactured for all of the GRC gearboxes.

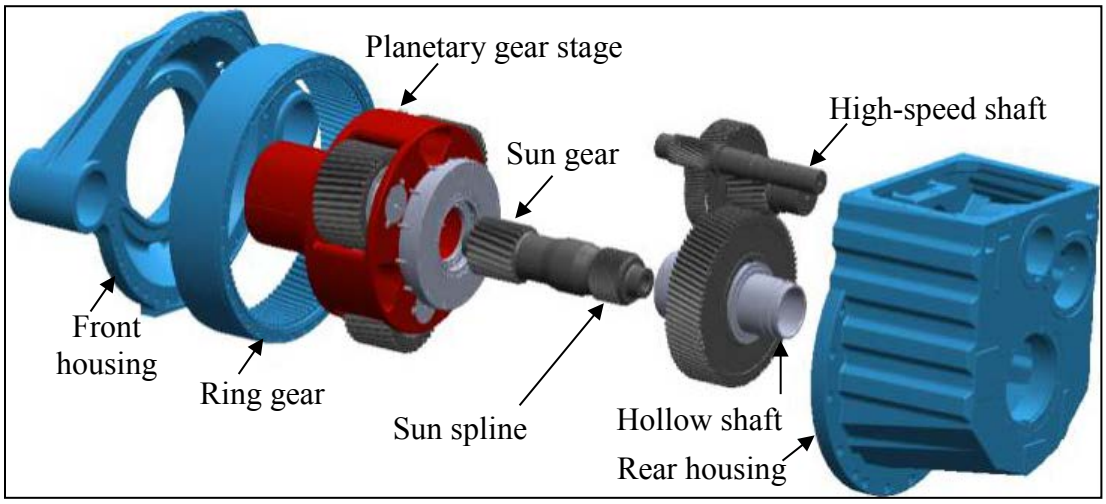

Figure 2. Gearbox configuration. *Illustration by Powertrain Engineers Inc.*

A tradeoff study was completed for the GB3 design to determine what planetary system changes had the most beneficial impact on predicted fatigue life [14-17]. After a down-selection process, which considered cost and schedule impacts, the following key improvements were selected:

- Preloaded planet carrier and planet TRBs, and stiffer planet pins to improve alignments in the planetary system and improve the load-sharing characteristics
- Planet TRB outer races integral to the planet gears to increase capacity and eliminate outer race fretting. The planet TRBs still utilize an inner race containing instrumentation, resulting in an overall semi-integrated planet bearing design

Additional design changes were also made to facilitate the key improvements, or otherwise improve assembly or operation of the gearbox. Although valuable, the following changes were not part of the test verification process:

- A robust bolt system between the ring gear and front and rear housings to accommodate increased axial loads from the planetary system
- A ring gear nitrided to improve fatigue life. The ring gear is also 29 mm longer to improve ease of assembly of the central plate and allow more space for the TRBs and the new oil feed ring system. This change necessitated shifting the generator aft by the same amount by enlarging the mounting holes in the generator-mount cross members
- The spline coupling crowning was reduced by 50% to increase the load-carrying area of the spline without negatively affecting system life or gear alignment
- Hollow shaft bearings in an X-arrangement with tighter inner races to reduce fretting
- An improved, semidry sump lubrication system with improved delivery to the planet bearings, planet gears, and HSS TRBs.

A comparison of the key characteristics of both GRC gearbox designs is shown in Figure 3.

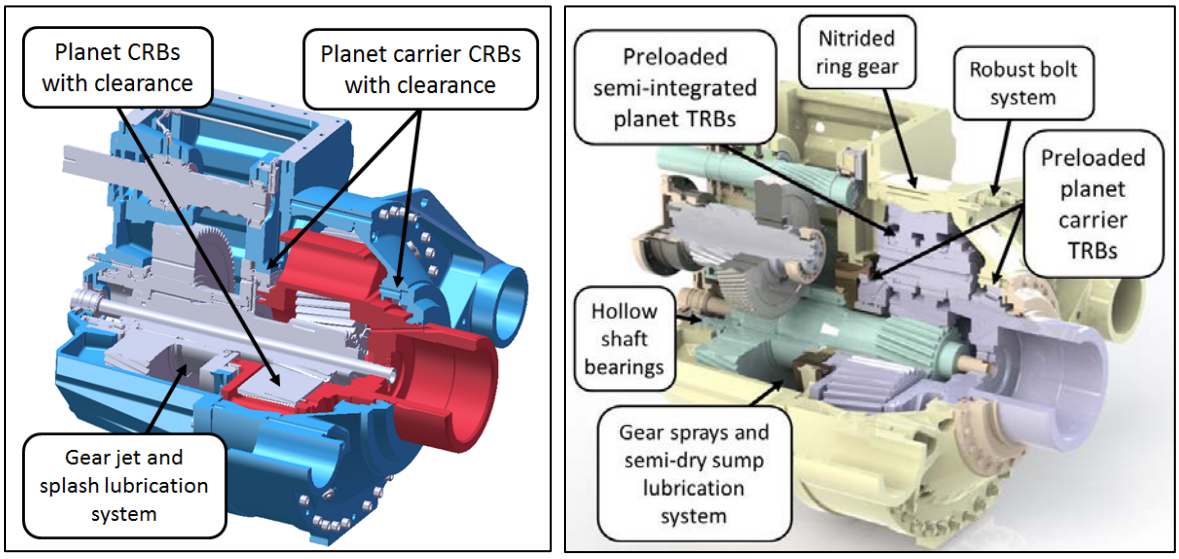

Figure 3. Comparison of GB2 (left) and GB3 (right) design characteristics. *Illustration by Romax Technology (right)*

3 Test Environment

The National Wind Technology Center (NWTC) 2.5-megawatt (MW) dynamometer test facility [21] was used for GB3 testing. The dynamometer variable frequency drive and NTL system enabled the reproduction of field conditions. The dynamometer variable frequency drive enables dynamic torque control up to a bandwidth of 250 hertz (Hz). The NTL system can apply thrust, vertical force, and lateral force to the adapter couplings in front of the GRC main bearing as shown in Figure 4. Given the fixed distance between the NTL application point and the GRC main bearing, the relationship between these vertical and lateral forces and the resulting pitch or yaw moments on the GRC main shaft is fixed and cannot be controlled independently. The NTL system can apply loads dynamically up to approximately 10 Hz, depending on force and hydraulic flow volume requirements. GB3 installed in the drivetrain is shown in Figure 5.

Figure 4. Drivetrain dynamometer installation. *Photo by Jonathan Keller, NREL 40428*

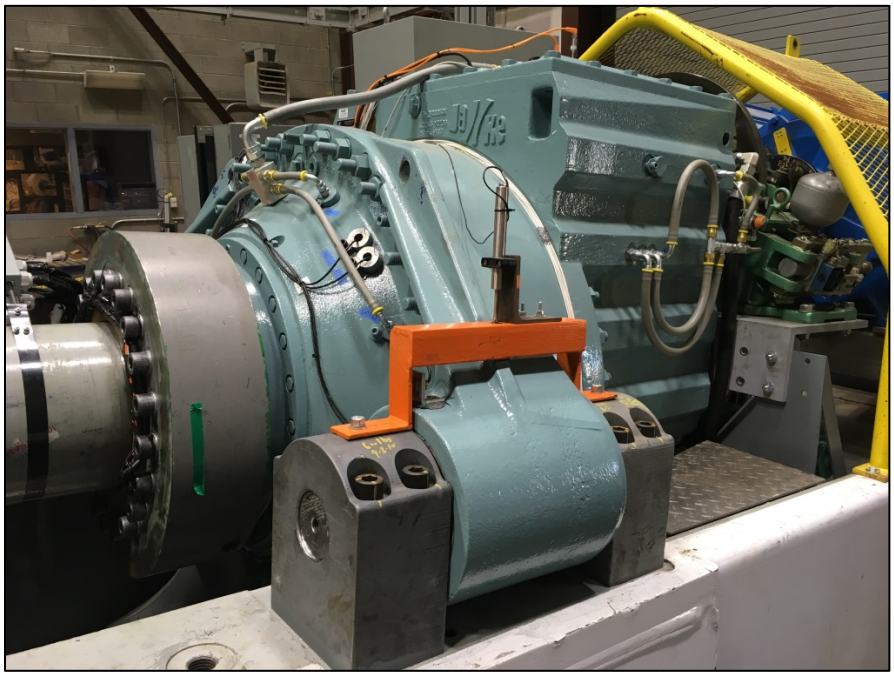

Figure 5. GB3 installation. *Photo by Jonathan Keller, NREL 40430*

The data acquisition system (DAS) was based on the National Instrument's deterministic Ethernet platform. One set of chassis processed rotating planetary section signals and was mounted in an enclosure on the main shaft. The output of that system was converted to fiber optic signals and sent back through the conduit tube in the center of the gearbox low-speed shaft. A fiber optic rotary joint at the rear of the gearbox then converted the signals to the nonrotating frame. A second set of chassis processed other fixed frame signals and all of the HSS signals. The DAS and chassis are shown in Figure 6.

Figure 6. Data acquisition system. *Photo by Mark McDade, NREL 40432*

4 Instrumentation

Detailed descriptions for all instrumentation are included in the test plan [19]. For reference, instrumentation for Phase 3 testing of GB3 is categorized by location of the sensor, as listed below.

- Dynamometer
- Nontorque loading system
- Main shaft
- Gearbox
    - Housing
    - Ring gear
    - Planet carrier
    - Planet gears
    - Planet bearings
    - Sun gear
    - Low-speed shaft (LSS) bearings
    - Intermediate-speed shaft bearings
    - High-speed shaft
    - High-speed shaft bearings
- Lubrication system
- Controller.

4.1 Instrumentation Changes and Deviations

After installation and initial commissioning, some deviations from the planned instrumentation were discovered. Those deviations are summarized here and, where necessary, described further in the following sections.

The zero-point of the main shaft azimuth measurement (signal name LSS_Azimuth) derived from an encoder installed on the fiber optic slip ring, the azimuthal location of the strain gages rotating on the main shaft (signal names MSBM_YY and MSBM_ZZ), and the azimuthal location of any planet do not coincide with each other. That is, each has an azimuthal offset that is best determined after the main shaft and encoder are installed to the gearbox. To determine these offsets, data was acquired while the gearbox was stationary and the planet and main shaft positions were examined. In this manner, the offset of the main shaft azimuth to the main shaft strain gages was determined to be $\phi_0 = 113°$. That is, the rotor bending moments in the fixed frame (signal names MSBM_y and MSBM_z) can be determined from the rotating measurements by

$$\begin{aligned} \text{MSBM\_y} &= -\text{MSBM\_YY}\sin\left(\text{LSS\_Azimuth} - \phi_0\right) - \text{MSBM\_ZZ}\cos\left(\text{LSS\_Azimuth} - \phi_0\right) \\ \text{MSBM\_z} &= +\text{MSBM\_YY}\cos\left(\text{LSS\_Azimuth} - \phi_0\right) - \text{MSBM\_ZZ}\sin\left(\text{LSS\_Azimuth} - \phi_0\right) \end{aligned} \quad (1)$$

Examining the stationary data set shows a negative fixed frame pitch moment, M_y = -69 kilonewton meter (kNm) and a near zero fixed frame yaw moment, M_z =1 kNm, confirming this offset. In this position, the measured main shaft azimuth was 56.3° and planet A was close to the top of the ring gear. By examining the strain at the top of the ring gear in operation, it was determined that the actual offset of planet A from the top of the ring gear is approximately 84°. That is, when the measured main shaft azimuth is 84°, planet A is at the 0° circumferential location, planet B is at the 240° location, and planet C is at the 120° location. Similarly, the HSS azimuth measurement (signal name HSS_Azimuth) also contains an offset because of its mounting. For both GB2 and GB3, the offset is 60° [6].

More notably, one of the planet bearing strain gages (signal name PlanetB_LOAD_DW_77) was not operational. Presumably, it was damaged during either the assembly, shipping, or installation process of the gearbox. Although nonoperational, it remained a part of the data stream. For curve fitting of the bearing load zone, it can reasonably be assumed that this measurement is the same value as the measurement on the opposite side of the load zone (signal name PlanetB_LOAD_DW_323) as illustrated in the next section. Additionally, two other strain gages on the same planet (signal names PlanetB_LOAD_DW_20 and PlanetB_LOAD_DW_285) appear to have been swapped or otherwise labeled incorrectly as shown in the next section. They retain their original, expected data labels in the data stream.

Additionally, the temperature measurements on the inner rings of the HSS bearings (signal names TEMP_HSS_TRB_IR_UW and TEMP_HSS_TRB_IR_DW), which are transmitted through a slip ring on the HSS, became highly variable and provided unrealistic values in the latter portion of testing. The strain gage measurements on the HSS did not seem to be affected, however. Lastly, the indicator of the generator's electrical connection to the grid at low power (signal name Controller_g_contactor) listed in the test plan was also not operational nor was it part of the data stream.

4.2 Signal List

Data was recorded in two separate data streams. A 100-Hz rate was used to record information on the planetary and intermediate sections of the gearbox. A 2,000-Hz rate was used to record information on the high-speed section of the gearbox. Relevant signals related to the input loading conditions, lubrication, or output performance of the generator and controller were also recorded. Many signals were measured in engineering units, whereas others were recorded in units of millivolts per volt (mV/V). The signals included in each data stream are listed in Table A-1 and Table A-2 in Appendix A, for the 100-Hz and 2,000-Hz rates, respectively.

The data files were named beginning with the convention "Test Type_," derived from the name of a particular test in the test plan such as "Static_NTL." "Test Sequence_" follows Test Type and corresponds to sequences in the test plan such as "5A." Finally, the data file names were appended with "YYYY_MM_DD_HH_SS_ZZZZHz.tdms," in which YYYY, MM, DD, HH, and SS are the year, month, date, hour, and second of the data acquisition, respectively, and ZZZZ is the acquisition rate in hertz.

5 Test Sequence

Testing of GB3 in Phase 3 consisted of the following major test sequences:

- Drivetrain recommissioning
- NTL tests
- HSS radial misalignment tests
- Field-representative tests
- Variable-speed tests.

5.1 Drivetrain Commissioning

The drivetrain commissioning test sequence ensured that the dynamometer controls, drivetrain, gearbox, lubrication and cooling systems, and instrumentation were all operating normally and ready for full-load testing. Throughout the commissioning process examples of data were reviewed and the instrumentation signals were corrected as necessary. Data sets were also gathered in nonoperational (static) states to record signal offsets. The gearbox first underwent flushing, followed by a break-in sequence during which the sensors and controls were verified while gradually increasing speed, torque, and nontorque loads.

5.1.1 Gearbox Flushing

Commissioning began on Sept. 14, 2016, by flushing the gearbox to remove contaminants that might have been left over from the manufacturing and assembly process. The gearbox oil was heated to over 45°C and the lubrication system was operated to flush the oil through the gearbox, small particle filter, and oil particle counter until it reached a cleanliness of -/14/11. The dynamometer was then engaged and the gearbox was spun at low speed (5% to 10% rated speed or 1 to 2 rpm) while continuing to flush the oil.

5.1.2 Gearbox Run-In

The objective of "running-in" the gearbox, listed in Table 1, was to reduce the roughness of mating surfaces created by the manufacturing process. The run-in procedure was completed between Sept. 14 and 19, 2016. During the process, inconsistencies in the torque and power signals were noted and corrected, requiring two separate runs in some cases.

Table 1. Gearbox Run-In Procedure

Date	Load Step	Drivetrain Speed (%)	Torque (%/kNm)	Duration (hr)	Oil Sump Temp (°C)	Oil Cleanliness
Sept. 14	1	30	5/18	1.0	43	-/14/10
Sept. 14-15	3	100	5/18	2.5	55	-/15/11
Sept. 16	4a	100	20/72	1.5	52	-/15/10
Sept. 16	5a	100	40/144	2.0	54	-/14/9
Sept. 16	6a	100	60/216	0.5	65	-/15/11
Sept. 16	7a	100	80/288	0.5	64	-/15/11
Sept. 16-19	8a-b	100	100/360	4.5	66	-/15/10

At each load step, the oil sump and bearing temperatures were stabilized and the oil cleanliness level were better than -/15/12. After the last load step, all oil filters were replaced.

5.1.3 High-Speed Shaft Torque Investigation

In previous testing of GB2, a periodic ±10% variation in the HSS torque was measured—even in offline conditions [6-7,10]. A possible source for this variation has been hypothesized as tooth spacing errors on the high-speed pinion [22]. Because the high-speed pinion was newly manufactured for GB3, there was an opportunity to examine this hypothesis by repeating previous GB2 testing. The test sequence listed in Table 2 was completed on Oct. 4, 2016.

Table 2. HSS Torque Investigation Tests

Date	Power (%/kW)	Drivetrain Speed (%)	HSS Speed (rpm)
Oct. 4	Offline	16.7	300
Oct. 4	Offline	33.3	600
Oct. 4	Offline	50	900
Oct. 4	Offline	66.7	1,200
Oct. 4	12%/90	66.7	1,200
Oct. 4	25%/188	66.7	1,200
Oct. 4	Offline	83.3	1,500
Oct. 4	Offline	100	1,800
Oct. 4	25%/188	100	1,800
Oct. 4	50%/375	100	1,800
Oct. 4	75%/563	100	1,800
Oct. 4	100%/750	100	1,800

HSS bending moments and torque can be calculated in an identical manner as GB2 testing [7], updated to reflect the gage factors and offsets in the data that are specific to GB3 [23].

$$M = \frac{\pi\left(D^4 - d^4\right)E}{32DG_M}\frac{dV}{V} = K_M\frac{dV}{V} + b_m \tag{2}$$

$$T = \frac{\pi\left(D^4 - d^4\right)E}{16DG_T\left(1+\upsilon\right)}\frac{dV}{V} = K_T\frac{dV}{V} + b_T \tag{3}$$

Updated dimensional and material characteristics of the HSS and instrumentation are listed in Table 3 and the resulting calibration coefficients and data offsets are listed in Table 4. Negative scale factors relate to particular wiring of the strain gage bridges. Bending moment offsets were determined by eliminating the average bending moment for the full power case, whereas the torque offset was determined from the static, nonoperational test data. The net torque calculated with this process is positive and is in terms of the torque that the HSS applies to the generator.

Table 3. HSS and Instrumentation Properties

Inner Diameter d (m)	Outer Diameter D (m)	Modulus of Elasticity E (GPa)	Poisson's Ratio υ	Bending Gage Factor G_M	Torque Gage Factor G_T
0.025	0.1	207	0.3	2.155	2.135

Table 4. HSS Bending and Torque Coefficients and Offsets

Signal	Scale Factor (kNm/mV/V)	Offset (kNm)
HSS_UY_BM	-9.399	-0.139
HSS_UZ_BM	9.399	0.079
HSS_DY_BM	-9.399	0.206
HSS_DZ_BM	9.399	0.004
HSS_exY_BM	-9.399	-0.327
HSS_exZ_BM	9.399	-0.383
HSS_TQ	-14.596	0.072

The measured torque data at rated speed for each gearbox is shown in Figure 7. In each condition, data was acquired over 30 shaft revolutions. Although the absolute torque levels for the gearboxes differ slightly, the overall pattern is clear. The HSS torque variation evident in GB2 has largely been eliminated in GB3.

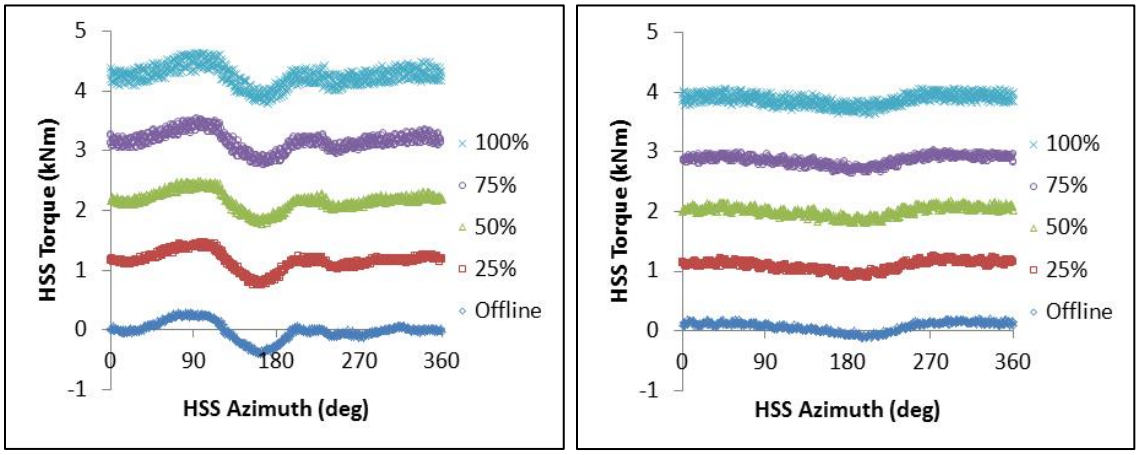

Figure 7. HSS torque at 1,800 rpm for GB2 (left) and GB3 (right)

5.2 Nontorque Load Tests

Phase 3 testing of GB3 repeated the sequence of NTL tests for direct comparison to GB2, with additional data acquisitions at high NTL levels to assess data repeatability. The NTL tests proceeded from simple static bending moments, through simple dynamic bending moments, to static thrust load testing. The following sections describe each test series.

5.2.1 Static Bending Moment

Static bending moment tests for GB3 were conducted in offline conditions (sequences 1–3), and at 25% power (sequence 4), 50% power (sequence 5), 75% power (sequence 6), and 100% power (sequence 7) conditions. Similar to testing on GB2, additional test data were acquired at 10% power in a final sequence (sequence 8). The operating conditions for these sequences are summarized in Table 5, which also references specific bending moment conditions provided in Table 6. The static bending tests were performed from Sept. 21 to Sept. 29, 2016.

Table 5. Static NTL Tests

Date	Test Number	Power (%)	Speed (%)	Rotation Direction	NTL Sequences
Sept. 21	1	Offline	5.5	Normal	A1,H1
Sept. 28	2	Offline	5.5	Reverse	A1,H1
Sept. 23	3	Offline	100	Normal	All
Sept. 26	4	25	100	Normal	All
Sept. 22	5	50	100	Normal	All
Sept. 28-29	6	75	100	Normal	All
Sept. 21	7	100	100	Normal	All
Sept. 22	8	10	100	Normal	A1,H1

Table 6. Static NTL Sequences

NTL Sequence	Myy (kNm)	Mzz (kNm)	Increment (kNm)
A1	-300 to 300	0	100
B	-300 to 300	-100	100
C	-300 to 300	-200	100
D	-300 to 300	-300	100
A2	-300 to 300	0	100
E	-300 to 300	100	100
F	-300 to 300	200	100
G	-300 to 300	300	100
A3	-300 to 300	0	100
H1	0	-300 to 300	100
H2	0	300 to -300	100

All cases were performed with respect to the tared (i.e., zero-bending-moment) condition, which changes slightly with drivetrain power. When tared, the pitch moment caused by the weight of the dynamometer couplings and shafting has been removed from the drivetrain. That is, tests with zero bending moment are in a pure-torque condition. Figure 8 shows an example of the test conditions that were achieved at rated power. Some of the most severe, combined pitch and yaw moment cases were not achieved because of overall limits of the actuator forces. These cases correspond to when the actuators must provide the vertical force required to first tare the drivetrain plus additional vertical or lateral forces required to achieve a large moment.

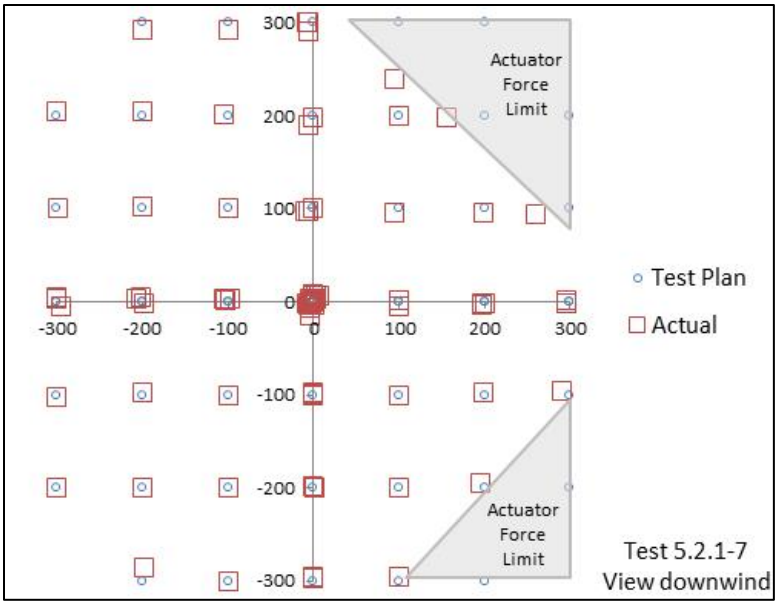

Figure 8. Static bending moments at 100% power

Three cycles of roller passages over several example planet B bearing strain gage measurements for the full-power, pure-torque case are shown in Figure 9 and Figure 10. Measured planet bearing strains can be converted to bearing load in kilonewton (kN) by examining the strain range along with the calibration factors that were measured in a special test rig [24]. The larger the strain range, the larger the bearing load at that measurement location. Offsets of each signal have been adjusted to make the strain range clearer.

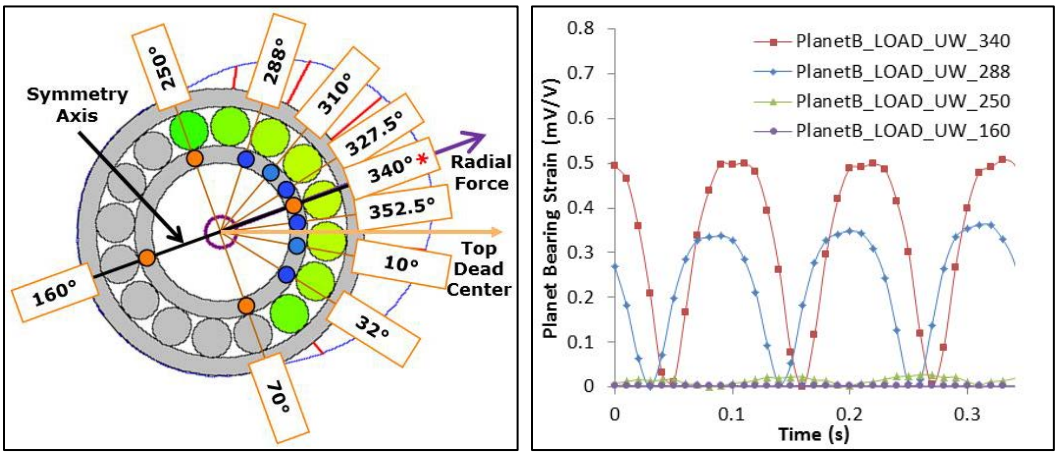

Figure 9. Planet B upwind bearing load zone (left) and measurements (right) at 100% power
Illustration by Timken (left)

For the upwind (UW) bearing, Figure 9 shows the highest loaded location at the expected center of the load zone (PlanetB_LOAD_UW_340) aligned with the radial force direction, a less loaded location in the outer half of the load zone (PlanetB_LOAD_UW_288), a very lightly loaded location at one of the edges of the expected load zone (PlanetB_LOAD_UW_250), and the unloaded location opposite the expected center of the load zone (PlanetB_LOAD_UW_160). The magnitudes of the resulting measurements are as expected; highest in the center of the load zone, much lower at the edges, and essentially zero opposite the load zone.

A similar example of the planet B downwind (DW) bearing strain gage measurements are also shown in Figure 10. Here, however, the measurement location at the expected center of the load zone (PlanetB_LOAD_DW_20) has a smaller magnitude than the other measurements in the load zone and the measurement location at the expected edge of the load zone (PlanetB_LOAD_DW_285) has the largest magnitude. By examining all the measurements for the planet B downwind bearing, the only reasonable explanation is that these two measurements were swapped. The unloaded location opposite the expected center of the load zone (PlanetB_LOAD_DW_200) has very little measured strain, as expected. Lastly, the two locations in the outer half of the load zone (PlanetB_LOAD_DW_323 and PlanetB_LOAD_DW_77) are also compared. These two measurements should be very similar in magnitude. However, upon further examination, one of them (PlanetB_LOAD_DW_77) has a value of exactly zero at all times in all acquisitions. Thus, for analysis purposes and curve fitting of the load zone this signal can be reasonably assumed to be equal to its counterpart (PlanetB_LOAD_DW_323). All analyses conducted hereafter assume this configuration as mentioned previously in Section 4.1.

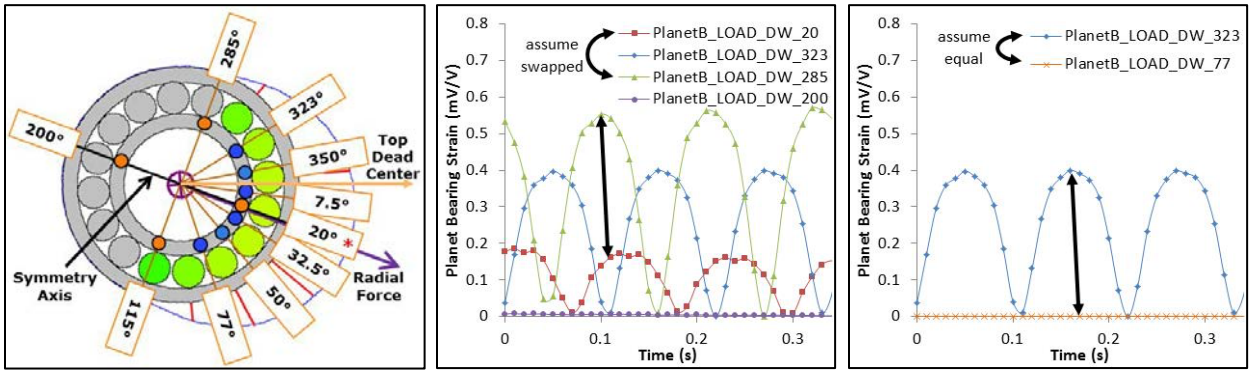

Figure 10. Planet B downwind bearing load zone (left) and measurements (center and right) at 100% power. *Illustration by Timken (left)*

5.2.2 Dynamic Bending Moment

Dynamic bending moment tests were completed in offline (sequence 1), 25%-power (sequence 2), and 100%-power (sequence 3) conditions on Oct. 21, 2016. The operating conditions for these sequences are summarized in Table 7, which also references specific NTL loading conditions provided in Table 8.

Table 7. Dynamic NTL Tests

Date	Test Number	Power (%)	Speed (%)	NTL Sequences
Oct. 21	1	Offline	100	All
Oct. 21	2	25	100	All
Oct. 21	3	100	100	All

Table 8. Dynamic NTL Sequences

NTL Sequence	Myy (kNm)	Mzz (kNm)	Frequency (Hz)
A	0 to -50	0	2
D	0 to -200	0	2
G	0	0 to 50	2
R	0	-100 to 100	2

5.2.3 Static Thrust

Static thrust test sequences were completed on Oct. 21, 2016, in offline mode (sequence 2), at 25%-power (sequence 3), 50%-power (sequence 4), 75%-power (sequence 5), and 100%-power (sequence 6) conditions as listed in Table 9.

Table 9. Static Thrust Tests

Date	Test Number	Power (%)	Speed (%)	Thrust (kN)	Increment (kN)
Oct. 21	2	Offline	100	0 to -100 to 100 to 0	50
Oct. 21	3	25	100	0 to -100 to 100 to 0	50
Oct. 21	4	50	100	0 to -100 to 100 to 0	50
Oct. 21	5	75	100	0 to -100 to 100 to 0	50
Oct. 21	6	100	100	0 to -100 to 100 to 0	50

5.3 Generator Misalignment Tests

New instrumentation on the GB3 HSS measures bearing temperature on the inner and outer rings of the TRB pair. The aligned and maximum misalignment (3º) conditions of the coupling shaft to the generator were tested in the offline mode (sequence 1 and 2), at 25%-power (sequence 3), 50%-power (sequence 4), 75%-power (sequence 5), and 100%-power (sequence 6) conditions listed in Table 10. Aligned tests were completed on Oct. 21, 2016, whereas misaligned tests were completed on Nov. 22, 2016.

Table 10. Generator Misalignment Tests

Test Number	Power (%)	Speed (%)	Misalignment (°/mm)
0	Offline	0	0/0 and 3°/32.06
1	Offline	5.5	0/0 and 3°/32.06
2	Offline	100	0/0 and 3°/32.06
3	25	100	0/0 and 3°/32.06
4	50	100	0/0 and 3°/32.06
5	75	100	0/0 and 3°/32.06
6	100	100	0/0 and 3°/32.06

Figure 11 shows the measured temperature differentials between the inner and outer rings for the HSS bearings over a range of drivetrain power settings. Because the downwind bearing carries both axial and radial load its temperature difference ranges between 20 and 27°C, higher than the 8–10°C temperature difference for the more lightly loaded upwind bearing. Bearing temperatures increase slightly with drivetrain power. The temperature of the oil at the bearing manifold was held nearly constant between 48.5 and 50°C by the oil cooling system. These measured temperature differentials are within the typical range given in the International Electrotechnical Commission's 61400-4 gearbox design standard. The results shown in Figure 11 were collected during the aligned tests on Oct. 21, 2016, whereas the inner ring measurements were consistent. Testing results after Oct. 21, 2016, display high variability and unrealistic values for the inner ring temperatures.

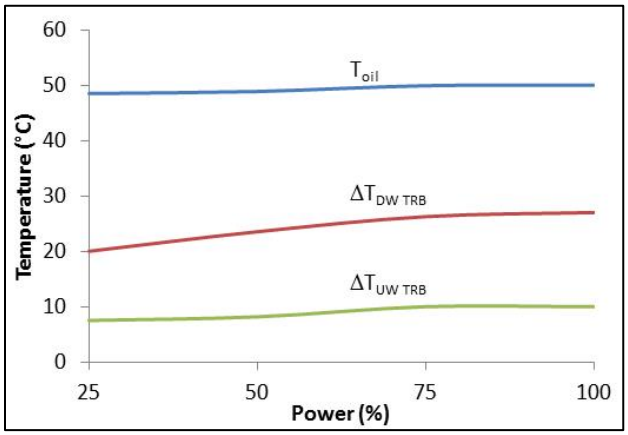

Figure 11. HSS bearing ring temperature differentials

5.4 Field-Representative Tests

Examples of field-representative testing completed in Phase 3 are discussed in the following sections. These examples correspond to normal power production and shutdown cases, respectively. Normal power production cases utilized the dynamometer variable-frequency drive and the dynamic capability of the NTL system, whereas the shutdown cases utilized the GRC drivetrain mechanical braking system.

5.4.1 Normal Power Production

Normal power production cases representing 5-meters per second (m/s), 15-m/s, and 25-m/s wind speed cases were tested. In each case, a system identification test was performed in which the desired dynamic torque is commanded and the actual torque is measured. This measured response is then used to tailor the commanded dynamic torque to result in a main shaft torque close to the values measured in the field. The NTLs were operated in force-feedback mode. The test for each wind speed case lasted 11 minutes, including a 30-second (s) ramp-up period to full load at the beginning of the test and a 30-s ramp-down period at the end of the test.

The normal power production cases were completed on Dec. 6, 2016. The tests proceeded in a graduated fashion, beginning with the low torque and NTLs for the 5-m/s wind speed case, then increasing them for the 15-m/s case, and increasing them again to near rated values for the 25-m/s case. A 10-s snapshot of the results for the 25-m/s wind speed case is shown in Figure 12.

The measured torque and bending moments in the dynamometer show good correlation with those measured in the field.

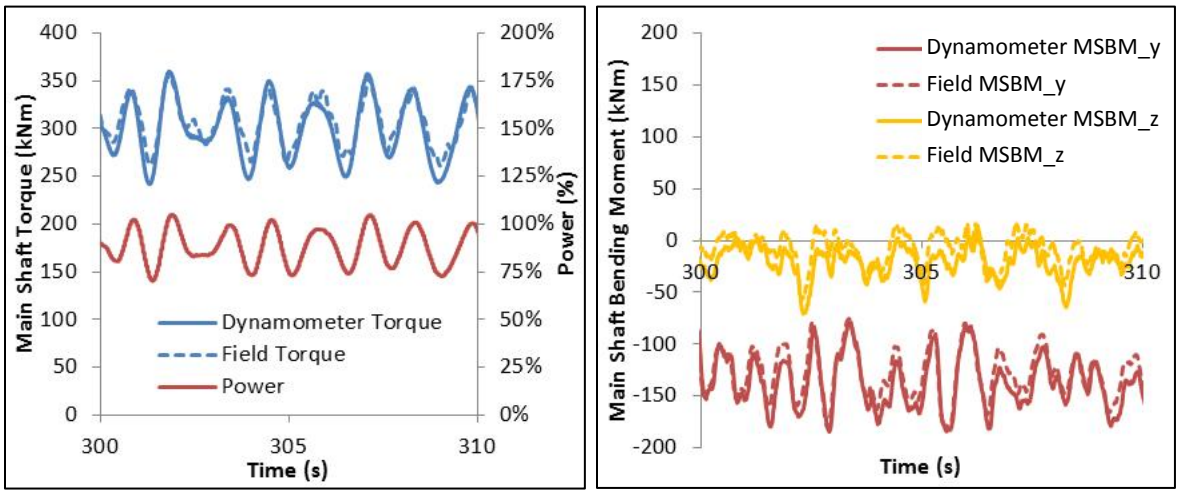

Figure 12. Main shaft torque (left) and bending moments (right) for the 25-m/s wind speed case

5.4.2 Shutdown

The GRC drivetrain uses a SIME-Stromag 3TWa37-TE2L single-caliper disk brake system. The brake disk is mounted with an interference fit to the end of the HSS. For the shutdown case, of primary interest are the loads reached immediately after engaging the disk brake.

Shutdown testing was completed on Nov. 3, 2016. The operation of the braking system hardware and software controls was verified in a graduated fashion. Each test was completed by operating the drivetrain at full speed with the generator offline, so that the initial torque was essentially zero. The power to the dynamometer was then cut off, and the system then began to slowly decelerate at a natural rate. The brake control system was programmed to actuate the brake calipers when the system crossed below a configurable speed, beginning with 1 rpm, and the resulting maximum torque value was measured. The brake application speed was then slowly increased over successive runs until the field speed of 11 rpm was reached, ensuring that the maximum torque did not exceed 200%. The final brake test in the dynamometer, where the torque reached 156% of rated, is compared in the right portion of Figure 13 to the field braking event, where the torque reached 160% of rated.

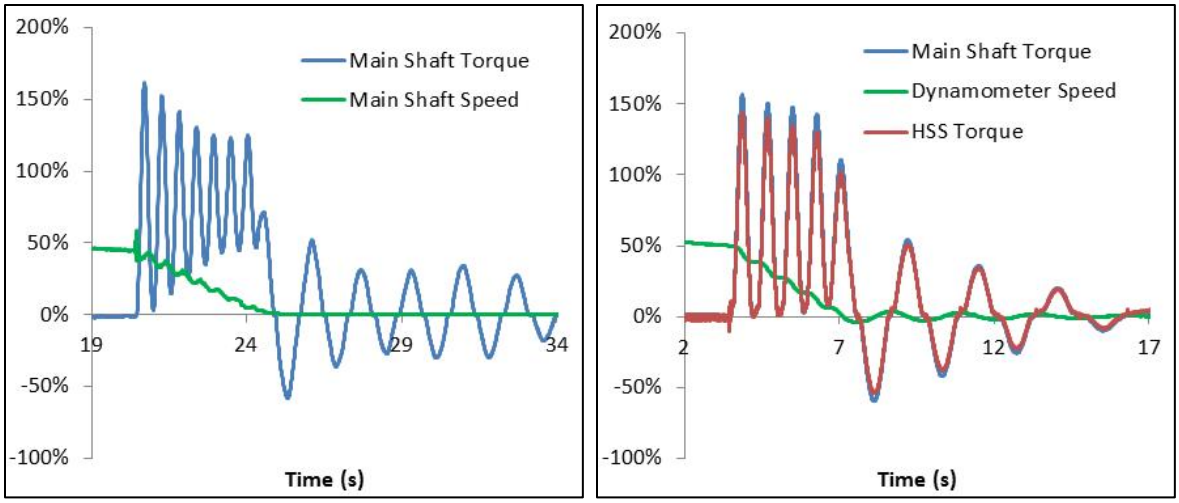

Figure 13. Shutdown event in the field (left) and dynamometer (right)

5.5 Grid Disconnect Tests

Controlled shutdown tests were also completed on Nov. 3, 2016. While operating at a steady-state power level, the dynamometer was intentionally shut down in a controlled fashion. The GRC generator immediately disconnects and the dynamometer ramps down at a controlled speed, taking about 3 minutes to come to a complete stop. Shutdowns were performed at 25% power, 50% power, 75% power, and 100% power levels. It should be noted that the behavior wherein the GRC controller immediately disconnects the generator from the grid is the same behavior the controller would exhibit in response to a grid event.

Example results for the shutdown from 100% power are shown in Figure 14 for 10 s of the event. At approximately 8 s, the shutdown began. The generator almost immediately disconnected, dropping to no power, and the dynamometer began a slow deceleration from full speed to approximately 85% speed at 16 s. The most interesting behavior was that of the torque data for both the main shaft and the HSS. When the generator was operating at rated power, the HSS was carrying the expected full torque. When the generator was disconnected, the torque quickly dropped and *reversed* to greater than 60% of rated and oscillated for multiple cycles, finally decaying to near zero torque at 16 s.

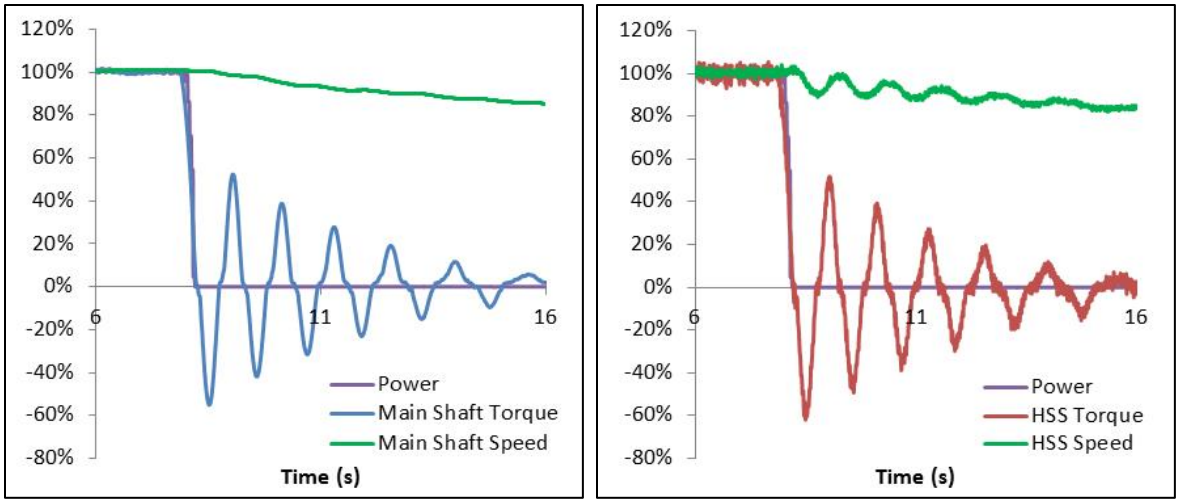

Figure 14. Main shaft (left) and HSS (right) response during controlled dynamometer shutdown

6 Summary

The GRC uses a combined testing, modeling, and analysis approach to investigate gearbox responses to specified loading conditions. Knowledge gained by comparing publicly available engineering models to measured data is disseminated to the industry, which facilitates gearbox reliability improvements. Ideally, the knowledge gained from the GRC will result in improvements to gearbox design standards and associated modeling tools.

This report describes the recent tests of the GRC GB3 in the NWTC's 2.5-MW dynamometer conducted during a few periods from September to December 2016. The primary test objective was to measure the planetary load-sharing characteristics in the same conditions as the original GRC gearbox design. If the measured load-sharing characteristics are close to the design model, the projected improvement in planetary section fatigue life and the efficacy of preloaded TRBs in mitigating the planetary bearing fatigue failure mode will have been demonstrated. The report serves as a guide for interpreting the publicly available data sets [20] with brief analyses to illustrate the tests and measured data. Detailed analysis of planetary load sharing characteristics will be presented in subsequent publications.

References

1. Sheng, S. 2013. *Report on Wind Turbine Subsystem Reliability—A Survey of Various Databases*. NREL/PR-5000-59111. National Renewable Energy Laboratory (NREL), Golden, CO (US). http://www.nrel.gov/docs/fy13osti/59111.pdf.

2. Link, H., W. LaCava, J. van Dam, B. McNiff, S. Sheng, R. Wallen, M. McDade, S. Lambert, S. Butterfield and F. Oyague. 2011. *Gearbox Reliability Collaborative Project Report: Findings from Phase 1 and Phase 2 Testing* (Technical Report). NREL/TP-5000-51885. National Renewable Energy Laboratory (NREL), Golden, CO (US). http://www.nrel.gov/docs/fy11osti/51885.pdf.

3. Guo, Y., J. Keller and W. LaCava. 2014. *Planetary gear load sharing of wind turbine drivetrains subjected to non-torque loads*. Wind Energy, 18 (4): 757–68. doi: 10.1002/we.1731.

4. Keller, J. and R. Wallen. 2015. *Gearbox Reliability Collaborative Phase 3 Gearbox 2 Test*. NREL/TP-5000-63693. National Renewable Energy Laboratory (NREL), Golden, CO (US). doi: 10.7799/1254154. https://doi.org/10.7799/1254154.

5. Link, H., J. Keller, Y. Guo and B. McNiff. 2013. *Gearbox Reliability Collaborative Phase 3 Gearbox 2 Test Plan*. (Technical Report). NREL/TP-5000-58190. National Renewable Energy Laboratory (NREL), Golden, CO (US). http://www.nrel.gov/docs/fy13osti/58190.pdf.

6. Keller, J. and R. Wallen. 2015. *Gearbox Reliability Collaborative Phase 3 Gearbox 2 Test Report* (Technical Report). NREL/TP-5000-63693. National Renewable Energy Laboratory (NREL), Golden, CO (US). http://www.nrel.gov/docs/fy15osti/63693.pdf.

7. Keller, J. and B. McNiff. 2014. *Gearbox Reliability Collaborative High-Speed Shaft Calibration* (Technical Report). NREL/TP-5000-62373. National Renewable Energy Laboratory (NREL), Golden, CO (US). http://www.nrel.gov/docs/fy14osti/62373.pdf.

8. Keller, J., Y. Guo and B. McNiff. 2013. *Gearbox Reliability Collaborative High Speed Shaft Tapered Roller Bearing Calibration* (Technical Report). NREL/TP-5000-60319. National Renewable Energy Laboratory (NREL), Golden, CO (US). http://www.nrel.gov/docs/fy14osti/60319.pdf

9. McNiff, B., Y. Guo, J. Keller and L. Sethuraman. 2014. *High-Speed Shaft Bearing Loads Testing and Modeling in the NREL Gearbox Reliability Collaborative: Preprint.* NREL/CP-5000-63277. National Renewable Energy Laboratory (NREL), Golden, CO (US). http://www.nrel.gov/docs/fy15osti/63277.pdf.

10. Keller, J., Y. Guo and L. Sethuraman. 2016. *Gearbox Reliability Collaborative Investigation of Gearbox Motion and High-Speed-Shaft Loads*. (Technical Report). NREL/TP-5000-65321. National Renewable Energy Laboratory (NREL), Golden, CO (US). http://www.nrel.gov/docs/fy16osti/65321.pdf.

11. Keller, J. and Y. Guo. 2016. *Gearbox Reliability Collaborative Investigation of High Speed Shaft Bearing Loads*. (Technical Report). NREL/TP-5000-66175. National Renewable Energy Laboratory (NREL), Golden, CO (US). http://www.nrel.gov/docs/fy16osti/66175.pdf.

12. Helsen, J., W. Weijtjens, Y. Guo, J. Keller, B. McNiff, C. Devriendt and P. Guillaume. 2015. *Experimental Characterization of a Grid-Loss Event on a 2.5-MW Dynamometer Using Advanced Operational Modal Analysis: Preprint.* (Technical Report). NREL/TP-5000-63501. National Renewable Energy Laboratory (NREL), Golden, CO (US). http://www.nrel.gov/docs/fy15osti/63501.pdf.

13. Helsen, J., Y. Guo, J. Keller and P. Guillaume. 2016. *Experimental Investigation of Bearing Slip in a Wind Turbine Gearbox during a Transient Grid Loss Event*. Wind Energy. doi: 10.1002/we.1979.

14. Keller, J., M. McDade, W. LaCava, Y. Guo and S. Sheng. 2012. *Gearbox Reliability Collaborative Update*. NREL/PR-5000-54558. National Renewable Energy Laboratory (NREL), Golden, CO (US). http://www.nrel.gov/docs/fy12osti/54558.pdf.

15. Sheng, S., J. Keller and C. Glinksy. 2013. *Gearbox Reliability Collaborative Update*. NREL/PR-5000-60141. National Renewable Energy Laboratory (NREL), Golden, CO (US). http://www.nrel.gov/docs/fy14osti/60141.pdf.

16. Keller, J. 2014. *Wind Turbine Drivetrain Testing and Research at the National Renewable Energy Laboratory*. NREL/PR-5000-62887. National Renewable Energy Laboratory (NREL), Golden, CO (US). http://www.nrel.gov/docs/fy15osti/62887.pdf.

17. Keller, J. 2015. *Gearbox Reliability Collaborative: Gearbox 3 Manufacturing Status*. NREL/PR-5000-63869. National Renewable Energy Laboratory (NREL), Golden, CO (US). http://www.nrel.gov/docs/fy15osti/63869.pdf.

18. National Renewable Energy Laboratory. 2013. *NREL Collaborative Improves the Reliability of Wind Turbine Gearboxes*. NREL/FS-6A42-59017. National Renewable Energy Laboratory (NREL), Golden, CO (US). http://www.nrel.gov/docs/fy13osti/59017.pdf.

19. Keller, J. and R. Wallen. 2017. Gearbox Reliability Collaborative Phase 3 Gearbox 3 Test Plan (Technical Report). NREL/TP-5000-66594. National Renewable Energy Laboratory (NREL), Golden, CO (US). http://www.nrel.gov/docs/fy17osti/66594.pdf.

20. Keller, J. and R. Wallen. 2017. *Gearbox Reliability Collaborative Phase 3 Gearbox 3 Test*. National Renewable Energy Laboratory (NREL), Golden, CO (US). doi: 10.7799/1337868. https://doi.org/10.7799/1337868.

21. National Renewable Energy Laboratory. 2010. *Dynamometer Testing*. NREL/FS-5000-45649. National Renewable Energy Laboratory (NREL), Golden, CO (US). http://www.nrel.gov/docs/fy11osti/45649.pdf.

22. Houser, D. R. “Causes of GRC High Speed Shaft Dynamic Torque Variations.” Presented at the NREL GRC meeting, Golden, CO, February 17–18, 2015.

23. Graeter, J. 2016. Verification Report: Installed Instrumentation Equipment at NREL NWTC. Romax Technology Report 1551-DC-004-A.

24. Keller, J. and D. Lucas. 2017. Gearbox Reliability Collaborative Gearbox 3 Planet Bearing Calibration (Technical Report). NREL/TP-5000-67370. National Renewable Energy Laboratory (NREL), Golden, CO (US). http://www.nrel.gov/docs/fy17osti/67370.pdf.

Appendix A. Data Elements

Table A-1. Elements of 100-Hz Sample Rate Data

Location	Nomenclature	Expanded Nomenclature	Units	Sensor(s)
DAS	MS Excel Timestamp	Time, MS Excel format, from Jan 1, 1900	days	DAS
DAS	LabVIEW Timestamp	Time, Labview format, from Jan 1, 1904	s	DAS
Dyno Motor	Dyno_Speed	Speed, dynamometer gearbox output converted from dynamometer motor	rpm	Calculated
Dyno GB	Dyno_Torque	Torque, dynamometer gearbox output torque spool	kNm	Strain gage
NTL	NTL_Port_Disp	Displacement, NTL port cylinder	mm	Proximity
NTL	NTL_Port_Force	Force, NTL port cylinder	kN	Load cell
NTL	NTL_Star_Disp	Displacement, NTL starboard cylinder	mm	Proximity
NTL	NTL_Star_Force	Force, NTL starboard cylinder	kN	Load cell
NTL	NTL_Thrust_Disp	Displacement, NTL thrust cylinder	mm	Proximity
NTL	NTL_Thrust_Force	Force, NTL thrust cylinder	kN	Load cell
Main shaft	LSS_TQ	Torque	kNm	Strain gage
Main shaft	MSBM_YY	Bending moment, rotating, y-axis	kNm	Strain gage
Main shaft	MSBM_ZZ	Bending moment, rotating, z-axis	kNm	Strain gage
Main shaft	MSBM	Bending moment, total	kNm	Calculated
Main shaft	MSBM_y	Bending moment, fixed, y-axis	kNm	Calculated
Main shaft	MSBM_z	Bending moment, fixed, z-axis	kNm	Calculated
Main shaft	LSS_Azimuth	Azimuth angle	degrees	Encoder
Main shaft	LSS_Speed	Shaft speed	rpm	Calculated
Housing	Trunion_Z_stbd	Displacement, gearbox Z starboard	mm	Proximity
Housing	Trunion_Z_port	Displacement, gearbox Z port	mm	Proximity
Housing	Trunion_My_bottom	Displacement, gearbox X bottom	mm	Proximity
Housing	Trunion_Y_port	Displacement, gearbox Y port	mm	Proximity

Location	Nomenclature	Expanded Nomenclature	Units	Sensor(s)
Housing	Trunion_X_stbd	Displacement, gearbox X starboard	mm	Proximity
Housing	Trunion_X_port	Displacement, gearbox X port	mm	Proximity
Housing	WEB_STRAIN_0	Strain in carrier web, 0° direction	mV/V	Strain gage
Housing	WEB_STRAIN_45	Strain in web, 45° direction	mV/V	Strain gage
Housing	WEB_STRAIN_315	Strain in web, 315° direction	mV/V	Strain gage
Ring gear	INT_KHB_0_A	Strain, ring gear teeth, 0° location	mV/V	Strain gage
Ring gear	INT_KHB_0_B	Strain, ring gear teeth, 0° location	mV/V	Strain gage
Ring gear	INT_KHB_0_C	Strain, ring gear teeth, 0° location	mV/V	Strain gage
Ring gear	INT_KHB_0_D	Strain, ring gear teeth, 0° location	mV/V	Strain gage
Ring gear	INT_KHB_0_E	Strain, ring gear teeth, 0° location	mV/V	Strain gage
Ring gear	INT_KHB_0_F	Strain, ring gear teeth, 0° location	mV/V	Strain gage
Ring gear	INT_KHB_0_G	Strain, ring gear teeth, 0° location	mV/V	Strain gage
Ring gear	INT_KHB_0_H	Strain, ring gear teeth, 0° location	mV/V	Strain gage
Ring gear	INT_KHB_120_A	Strain, ring gear teeth, 120° location	mV/V	Strain gage
Ring gear	INT_KHB_120_B	Strain, ring gear teeth, 120° location	mV/V	Strain gage
Ring gear	INT_KHB_120_C	Strain, ring gear teeth, 120° location	mV/V	Strain gage
Ring gear	INT_KHB_120_D	Strain, ring gear teeth, 120° location	mV/V	Strain gage
Ring gear	INT_KHB_120_E	Strain, ring gear teeth, 120° location	mV/V	Strain gage
Ring gear	INT_KHB_120_F	Strain, ring gear teeth, 120° location	mV/V	Strain gage
Ring gear	INT_KHB_120_G	Strain, ring gear teeth, 120° location	mV/V	Strain gage
Ring gear	INT_KHB_120_H	Strain, ring gear teeth, 120° location	mV/V	Strain gage
Ring gear	INT_KHB_240_A	Strain, ring gear teeth, 240° location	mV/V	Strain gage
Ring gear	INT_KHB_240_B	Strain, ring gear teeth, 240° location	mV/V	Strain gage
Ring gear	INT_KHB_240_C	Strain, ring gear teeth, 240° location	mV/V	Strain gage
Ring gear	INT_KHB_240_D	Strain, ring gear teeth, 240° location	mV/V	Strain gage

Location	Nomenclature	Expanded Nomenclature	Units	Sensor(s)
Ring gear	INT_KHB_240_E	Strain, ring gear teeth, 240° location	mV/V	Strain gage
Ring gear	INT_KHB_240_F	Strain, ring gear teeth, 240° location	mV/V	Strain gage
Ring gear	INT_KHB_240_G	Strain, ring gear teeth, 240° location	mV/V	Strain gage
Ring gear	INT_KHB_240_H	Strain, ring gear teeth, 240° location	mV/V	Strain gage
Ring gear	EXT_KHB_0_A	Strain, ring gear exterior, 0° location	mV/V	Strain gage
Ring gear	EXT_KHB_0_B	Strain, ring gear exterior, 0° location	mV/V	Strain gage
Ring gear	EXT_KHB_0_C	Strain, ring gear exterior, 0° location	mV/V	Strain gage
Ring gear	EXT_KHB_0_D	Strain, ring gear exterior, 0° location	mV/V	Strain gage
Ring gear	EXT_KHB_0_E	Strain, ring gear exterior, 0° location	mV/V	Strain gage
Ring gear	EXT_KHB_0_F	Strain, ring gear exterior, 0° location	mV/V	Strain gage
Ring gear	EXT_KHB_0_G	Strain, ring gear exterior, 0° location	mV/V	Strain gage
Ring gear	EXT_KHB_0_H	Strain, ring gear exterior, 0° location	mV/V	Strain gage
Ring gear	EXT_KHB_120_A	Strain, ring gear exterior, 120° location	mV/V	Strain gage
Ring gear	EXT_KHB_120_B	Strain, ring gear exterior, 120° location	mV/V	Strain gage
Ring gear	EXT_KHB_120_C	Strain, ring gear exterior, 120° location	mV/V	Strain gage
Ring gear	EXT_KHB_120_D	Strain, ring gear exterior, 120° location	mV/V	Strain gage
Ring gear	EXT_KHB_120_E	Strain, ring gear exterior, 120° location	mV/V	Strain gage
Ring gear	EXT_KHB_120_F	Strain, ring gear exterior, 120° location	mV/V	Strain gage
Ring gear	EXT_KHB_120_G	Strain, ring gear exterior, 120° location	mV/V	Strain gage
Ring gear	EXT_KHB_120_H	Strain, ring gear exterior, 120° location	mV/V	Strain gage
Ring gear	EXT_KHB_240_A	Strain, ring gear exterior, 240° location	mV/V	Strain gage
Ring gear	EXT_KHB_240_B	Strain, ring gear exterior, 240° location	mV/V	Strain gage
Ring gear	EXT_KHB_240_C	Strain, ring gear exterior, 240° location	mV/V	Strain gage
Ring gear	EXT_KHB_240_D	Strain, ring gear exterior, 240° location	mV/V	Strain gage
Ring gear	EXT_KHB_240_E	Strain, ring gear exterior, 240° location	mV/V	Strain gage

Location	Nomenclature	Expanded Nomenclature	Units	Sensor(s)
Ring gear	EXT_KHB_240_F	Strain, ring gear exterior, 240° location	mV/V	Strain gage
Ring gear	EXT_KHB_240_G	Strain, ring gear exterior, 240° location	mV/V	Strain gage
Ring gear	EXT_KHB_240_H	Strain, ring gear exterior, 240° location	mV/V	Strain gage
Carrier	Carrier_047	Displacement, carrier, X direction, 047°	mm	Proximity
Carrier	Carrier_137	Displacement, carrier, X direction, 137°	mm	Proximity
Carrier	Carrier_227	Displacement, carrier, X direction, 227°	mm	Proximity
Carrier	Carrier_317	Displacement, carrier, X direction, 317°	mm	Proximity
Carrier	Radial_040	Displacement Radial 40°	mm	Proximity
Carrier	Radial_310	Displacement Radial 310°	mm	Proximity
Planet	PlanetB_Rim_0	Displacement, X direction, 0°	mm	Proximity
Planet	PlanetB_Rim_90	Displacement, X direction, 90°	mm	Proximity
Planet	PlanetB_Rim_180	Displacement, X direction, 180°	mm	Proximity
Planet	PlanetC_Rim_0	Displacement, X direction, 0°	mm	Proximity
Planet	PlanetC_Rim_90	Displacement, X direction, 90°	mm	Proximity
Planet	PlanetC_Rim_180	Displacement, X direction, 180°	mm	Proximity
Planet	PlanetA_LOAD_UW_70	Strain, Planet A, upwind bearing, 70°	mV/V	Strain gage
Planet	PlanetA_LOAD_UW_160	Strain, Planet A, upwind bearing, 160°	mV/V	Strain gage
Planet	PlanetA_LOAD_UW_250	Strain, Planet A, upwind bearing, 250°	mV/V	Strain gage
Planet	PlanetA_LOAD_UW_340	Strain, Planet A, upwind bearing, 340°	mV/V	Strain gage
Planet	PlanetA_LOAD_DW_20	Strain, Planet A, downwind bearing, 20°	mV/V	Strain gage
Planet	PlanetA_LOAD_DW_115	Strain, Planet A, downwind bearing, 115°	mV/V	Strain gage
Planet	PlanetA_LOAD_DW_200	Strain, Planet A, downwind bearing, 200°	mV/V	Strain gage
Planet	PlanetA_LOAD_DW_285	Strain, Planet A, downwind bearing, 285°	mV/V	Strain gage
Planet	PlanetA_TEMP_UW_OUT1	Temperature, Planet A, upwind bearing, 340°	°C	Thermocouple
Planet	PlanetA_TEMP_UW_IN1	Temperature, Planet A, upwind bearing, 340°	°C	Thermocouple

Location	Nomenclature	Expanded Nomenclature	Units	Sensor(s)
Planet	PlanetA_TEMP_DW_IN1	Temperature, Planet A, downwind bearing, 20°	°C	Thermocouple
Planet	PlanetA_TEMP_DW_OUT1	Temperature, Planet A, downwind bearing, 20°	°C	Thermocouple
Planet	PlanetB_LOAD_UW_10	Strain, Planet B, upwind bearing, 10°	mV/V	Strain gage
Planet	PlanetB_LOAD_UW_32	Strain, Planet B, upwind bearing, 32°	mV/V	Strain gage
Planet	PlanetB_LOAD_UW_70	Strain, Planet B, upwind bearing, 70°	mV/V	Strain gage
Planet	PlanetB_LOAD_UW_160	Strain, Planet B, upwind bearing, 160°	mV/V	Strain gage
Planet	PlanetB_LOAD_UW_250	Strain, Planet B, upwind bearing, 250°	mV/V	Strain gage
Planet	PlanetB_LOAD_UW_288	Strain, Planet B, upwind bearing, 288°	mV/V	Strain gage
Planet	PlanetB_LOAD_UW_310	Strain, Planet B, upwind bearing, 310°	mV/V	Strain gage
Planet	PlanetB_LOAD_UW_327.5	Strain, Planet B, upwind bearing, 327.5°	mV/V	Strain gage
Planet	PlanetB_LOAD_UW_340	Strain, Planet B, upwind bearing, 340°	mV/V	Strain gage
Planet	PlanetB_LOAD_UW_352.5	Strain, Planet B, upwind bearing, 352.5°	mV/V	Strain gage
Planet	PlanetB_LOAD_DW_7.5	Strain, Planet B, downwind bearing, 7.5°	mV/V	Strain gage
Planet	PlanetB_LOAD_DW_20	Strain, Planet B, downwind bearing, 20° (assumed to actually be PlanetB_LOAD_DW_285)	mV/V	Strain gage
Planet	PlanetB_LOAD_DW_32.5	Strain, Planet B, downwind bearing, 32.5°	mV/V	Strain gage
Planet	PlanetB_LOAD_DW_50	Strain, Planet B, downwind bearing, 50°	mV/V	Strain gage
Planet	PlanetB_LOAD_DW_77	Strain, Planet B, downwind bearing, 77° (non-operational, assumed equal to PlanetB_LOAD_DW_323)	mV/V	Strain gage
Planet	PlanetB_LOAD_DW_115	Strain, Planet B, downwind bearing, 115°	mV/V	Strain gage
Planet	PlanetB_LOAD_DW_200	Strain, Planet B, downwind bearing, 200°	mV/V	Strain gage
Planet	PlanetB_LOAD_DW_285	Strain, Planet B, downwind bearing, 285° (assumed to actually be PlanetB_LOAD_DW_20)	mV/V	Strain gage
Planet	PlanetB_LOAD_DW_323	Strain, Planet B, downwind bearing, 323°	mV/V	Strain gage
Planet	PlanetB_LOAD_DW_350	Strain, Planet B, downwind bearing, 350°	mV/V	Strain gage
Planet	PlanetB_TEMP_UW_OUT1	Temperature, Planet B, upwind bearing, 340°	°C	Thermocouple

Location	Nomenclature	Expanded Nomenclature	Units	Sensor(s)
Planet	PlanetB_TEMP_UW_IN1	Temperature, Planet B, upwind bearing, 340°	°C	Thermocouple
Planet	PlanetB_TEMP_DW_IN1	Temperature, Planet B, downwind bearing, 20°	°C	Thermocouple
Planet	PlanetB_TEMP_DW_OUT2	Temperature, Planet B, downwind bearing, 20°	°C	Thermocouple
Planet	PlanetC_LOAD_UW_70	Strain, Planet C, upwind bearing, 70°	mV/V	Strain gage
Planet	PlanetC_LOAD_UW_160	Strain, Planet C, upwind bearing, 160°	mV/V	Strain gage
Planet	PlanetC_LOAD_UW_250	Strain, Planet C, upwind bearing, 250°	mV/V	Strain gage
Planet	PlanetC_LOAD_UW_340	Strain, Planet C, upwind bearing, 340°	mV/V	Strain gage
Planet	PlanetC_LOAD_DW_20	Strain, Planet C, downwind bearing, 20°	mV/V	Strain gage
Planet	PlanetC_LOAD_DW_115	Strain, Planet C, downwind bearing, 115°	mV/V	Strain gage
Planet	PlanetC_LOAD_DW_200	Strain, Planet C, downwind bearing, 200°	mV/V	Strain gage
Planet	PlanetC_LOAD_DW_285	Strain, Planet C, downwind bearing, 285°	mV/V	Strain gage
Planet	PlanetC_TEMP_UW_OUT1	Temperature, Planet C, upwind bearing, 340°	°C	Thermocouple
Planet	PlanetC_TEMP_UW_IN1	Temperature, Planet C, upwind bearing, 340°	°C	Thermocouple
Planet	PlanetC_TEMP_DW_IN1	Temperature, Planet C, downwind bearing, 20°	°C	Thermocouple
Planet	PlanetC_TEMP_DW_OUT1	Temperature, Planet C, downwind bearing, 20°	°C	Thermocouple
Sun	Sun_radial_ZZ	Displacement, radial, Z direction	mm	Proximity
Sun	Sun_radial_YY	Displacement, radial, Y direction	mm	Proximity
LSS	Temp_LSS_DW_BRG	Temperature, outer race	°C	RTD
ISS	Temp_ISS_DW_BRG	Temperature, outer race	°C	RTD
HSS	HSS_Speed	Shaft speed	rpm	Calculated
HSS	HSS_Azimuth	Azimuth angle	degrees	Encoder
HSS	HSS_TQ	Torque	mV/V	Strain gage
HSS	TEMP_HSS_TRB_IR_UW	Temperature, upwind TRB inner ring (poor data quality after October 21, 2016)	°C	RTD
HSS	TEMP_HSS_TRB_IR_DW	Temperature, downwind TRB inner ring (poor data quality after October 21, 2016)	°C	RTD

Location	Nomenclature	Expanded Nomenclature	Units	Sensor(s)
HSS	TEMP_HSS_TRB_OR_UW	Temperature, upwind TRB outer ring	°C	RTD
HSS	TEMP_HSS_TRB_OR_DW	Temperature, downwind TRB outer ring	°C	RTD
Lube System	ISO_OIL_CLEAN	Oil cleanliness, raw signal	-	CSM 1220
Lube System	ISO_1	Oil cleanliness, bin 1	-	Calculated
Lube System	ISO_2	Oil cleanliness, bin 2	-	Calculated
Lube System	ISO_3	Oil cleanliness, bin 3	-	Calculated
Lube System	Lube_Flow_Pump	Flow rate, total, at lube pump	lpm	Fan speed
Lube System	Lube_Return_Temp	Temperature, oil at main pump	°C	RTD
Lube System	Lube_Flow_Meter	Flow rate, to gearbox, at lube pump	lpm	Flow meter
Lube System	Lube_Fan_Speed	Speed, lube system fan	rpm	Fan speed
Lube System	Lube_Manifold_Pressure	Pressure, oil at distribution manifold	psi	Pressure
Lube System	Lube_Manifold_Temp	Temperature, oil at distribution manifold	°C	RTD
Lube System	Sump_Temp	Temperature, oil in gearbox sump	°C	RTD
Controller	Controller_G_contactor	Large-generator contactor	-	Relay
Controller	Controller_bypass_contactor	Soft-start bypass contactor	-	Relay
Controller	kW	Power, real	kW	Transformer
Controller	kVAR	Power, reactive	kVAR	Transformer

Table A-2. Elements of 2,000-Hz Sample Rate Data

Location	Nomenclature	Expanded Nomenclature	Units	Sensor(s)
DAS	MS Excel Timestamp	Time, MS Excel format, from Jan 1, 1900	days	DAS
DAS	LabVIEW Timestamp	Time, Labview format, from Jan 1, 1904	s	DAS
Dyno Motor	Dyno_Speed	Speed, dynamometer gearbox output converted from dynamometer motor	rpm	Calculated
Dyno GB	Dyno_Torque	Torque, dynamometer gearbox output torque spool	kNm	Strain gage
Main shaft	LSS_TQ	Torque	kNm	Strain gage
Main shaft	MSBM_YY	Bending moment, rotating, y-axis	kNm	Strain gage
Main shaft	MSBM_ZZ	Bending moment, rotating, z-axis	kNm	Strain gage
Main shaft	MSBM	Bending moment, total	kNm	Calculated
Main shaft	MSBM_yy	Bending moment, fixed, y-axis	kNm	Calculated
Main shaft	MSBM_zz	Bending moment, fixed, z-axis	kNm	Calculated
Main shaft	LSS_Azimuth	Azimuth angle	degrees	Encoder
Main shaft	LSS_Speed	Shaft speed	rpm	Calculated
HSS	HSS_UY_BM	Bending moment, upwind of mesh, rotating, y-axis	mV/V	Strain gage
HSS	HSS_UZ_BM	Bending moment, upwind of mesh, rotating, z-axis	mV/V	Strain gage
HSS	HSS_DY_BM	Bending moment, downwind of mesh, rotating, y-axis	mV/V	Strain gage
HSS	HSS_DZ_BM	Bending moment, downwind of mesh, rotating, z-axis	mV/V	Strain gage
HSS	HSS_exY_BM	Bending moment, downwind of bearings, rotating, y-axis	mV/V	Strain gage
HSS	HSS_exZ_BM	Bending moment, downwind of bearings, rotating, z-axis	mV/V	Strain gage
HSS	HSS_TQ	Torque	mV/V	Strain gage
HSS	TEMP_HSS_TRB_IR_UW	Temperature, upwind TRB inner ring (poor data quality after October 21, 2016)	°C	RTD
HSS	TEMP_HSS_TRB_IR_DW	Temperature, downwind TRB inner ring (poor data quality after October 21, 2016)	°C	RTD
HSS	TEMP_HSS_TRB_OR_UW	Temperature, upwind TRB outer ring	°C	RTD

Location	Nomenclature	Expanded Nomenclature	Units	Sensor(s)
HSS	TEMP_HSS_TRB_OR_DW	Temperature, downwind TRB outer ring	°C	RTD
HSS	HSS_Speed	Shaft speed	rpm	Calculated
HSS	HSS_Azimuth	Azimuth angle	degrees	Encoder
Controller	Controller_G_contactor	Large-generator contactor	-	Relay
Controller	Controller_bypass_contactor	Soft-start bypass contactor	-	Relay
Controller	kW	Power, real	kW	Transformer
Controller	kVAR	Power, reactive	kVAR	Transformer